Supplemental Data

Motor- and Tail-Dependent Targeting of Dynein to Microtubule Plus Ends and the Cell Cortex

Steven M. Markus, Jesse J. Punch, and Wei-Lih Lee

Supplemental Experimental Procedures

Plasmid construction

We constructed two targeting vectors designed to replace the chromosomal *DYN1* gene with fragments encoding for the tail and motor domains fused to three tandem GFP or YFP, respectively. We first built a plasmid containing 250 bp of the *DYN1* upstream and downstream non-coding regions. Briefly, a PCR fragment containing 250 bp upstream of the start codon of *DYN1* was amplified from genomic DNA using a forward primer flanked with a BglII site and a reverse primer flanked with SalI and BamHI sites. This fragment was digested with BglII and BamHI and ligated into BamHI-digested pBS-3GFP-TRP1 [22], yielding a plasmid containing 250 bp of the *DYN1* upstream non-coding sequence in front of *3GFP*. Next, a KpnI fragment containing 250 bp downstream of the stop codon of *DYN1* was amplified from genomic DNA and cloned into the unique KpnI site downstream of *3GFP* and *TRP1*, yielding pSM01. We verified both of the 250 bp fragments by sequencing. An engineered XhoI-SalI fragment encoding $Dyn1_{1\text{-}1363}$ ('tail' domain) was amplified from genomic DNA, digested with XhoI and SalI and ligated into the SalI site in pSM07 (a shuttle vector derived from pSM01), fusing *3GFP* to the 3' end of the cloned tail insert. The tail domain

was verified by DNA sequencing and was separated from *3GFP* by a linker sequence encoding ValAspGlySer. Next, a NotI fragment containing the *TAIL-3GFP* sequence was subcloned into the NotI site of the yeast vector pRS315 [37]. To remove extraneous DNA sequence (derived from pSM07 shuttle vector) between the 5' NotI site and the start codon of the tail domain sequence, we amplified a region of the cloned tail insert corresponding to nucleotides 1-599 of the *DYN1* gene using a forward primer flanked with a XhoI site. The PCR product was digested with XhoI and BglII (which was present at the 3' end of this amplified *DYN1* fragment) and was used to replace the XhoI-BglII fragment in the pRS315 vector carrying the *TAIL-3GFP* insert (the XhoI site was present in the multiple cloning sites of pRS315), yielding pRS315:*TAIL-3GFP*. Next, a XhoI-NotI fragment containing the *TAIL-3GFP* open reading frame was subcloned into the SalI and NotI sites of pSM01 to yield pSM01:*TAIL-3GFP*.

An engineered NotI fragment encoding $Dyn1_{1364\text{-}4092}$ ('motor' domain)-3YFP was amplified from genomic DNA isolated from a *DYN1-3YFP* yeast strain (YWL271) [17]. This fragment was digested with NotI and ligated into the yeast shuttle vector pRS306 [37]. To create an in-frame start codon and a desired restriction site, a region in the cloned insert corresponding to nucleotides 4092–7748 of the *DYN1* gene was amplified using a forward primer flanked with a XhoI site and a start codon. The PCR product was digested with XhoI and AvrII (which was present at the 3' end of this amplified *DYN1* fragment), and was used to replace the XhoI-AvrII fragment in the above pRS306 vector containing the *MOTOR-3YFP* insert. The resulting plasmid, pRS306:*MOTOR-3YFP*, contained a start codon followed by the wild-type coding sequence of the motor domain fused in-frame to *3YFP*. The motor domain was verified by DNA sequencing. Next, a

XhoI-NotI fragment containing the *MOTOR-3YFP* open reading frame was subcloned into the SalI and NotI sites in pSM01, yielding pSM01:*MOTOR-3YFP*. The same XhoI-NotI fragment was also ligated into pRS315 digested with XhoI and NotI to yield pRS315:*MOTOR-3YFP*. Site-directed mutagenesis of the motor domain was performed in pRS315:*MOTOR-3YFP* as described [38], and verified by sequencing. Resulting mutants were subcloned from pRS315:*MOTOR-3YFP* into pSM01, as above. Using similar methods, the K2424A point mutation was introduced into full-length *DYN1* in a targeting vector to yield pSM07:$DYN1_{K2424A}$-*3YFP*.

To drive the inducible expression of *TAIL-3GFP* or *MOTOR-3YFP* in the pRS315 CEN vector, an engineered SalI fragment containing the *MET3* promoter was amplified from pAFS92 (a gift from Jeff Moore, Washington University School of Medicine). This fragment was digested with SalI and ligated into pRS315:*TAIL-3GFP*, pRS315:*MOTOR-3YFP* or pRS315 digested with XhoI, to yield pRS315-*MET3*p:*TAIL-3GFP*, pRS315-*MET3*p:*MOTOR-3YFP*, or pRS315-*MET3p*. To generate pRS315-*MET3p*:*3GFP*, the *3GFP* open reading frame was subcloned as a BamHI-NotI fragment from pSM01 and ligated into pRS315-*MET3p* digested with BamHI and NotI.

To produce mCherry, 2mCherry and 3mCherry tagging vectors, an engineered BamHI-BglII *mCherry* fragment was amplified from pAK011 (a gift from E. Schiebel, Zentrum fur Molekulare Biologie der Universität Heidelberg, Heidelberg, Germany), digested with BamHI and BglII and ligated into pRS305 digested with BamHI to yield pRS305:*mCherry*. A second *mCherry* open reading frame minus the stop codon with engineered N-terminal linker sequence (MetValSerLysGlyGluGlu), a 5' BamHI site, and 3' AvrII and BamHI sites was amplified from pRS305:*mCherry*. This product was

digested with BamHI and ligated into pRS305:*mCherry* digested with BamHI to yield pRS305:*2mCherry*. To produce pRS305:*3mCherry*, a third AvrII-SpeI engineered *mCherry* fragment, also without a stop codon, was amplified by PCR from pRS305:*mCherry*, digested with AvrII and SpeI and ligated into pRS305:*2mCherry* digested with AvrII to yield pRS305:*3mCherry*. BamHI-NotI *mCherry*, *2mCherry* and *3mCherry* fragments were subcloned from pRS305 into pRS303 digested with BamHI and NotI, yielding pRS303:*mCherry*, pRS303:*2mCherry* and pRS303:*3mCherry*. These plasmids were used as templates for PCR-mediated tagging of chromosomal genes to create *NUM1-mCherry*::*LEU2* (YWL644 and YWL843), *DYN1-2mCherry::HIS3* (YWL731), *DYN1-3mCherry::HIS3* (YWL898) and *JNM1-3mCherry::HIS3* (YWL869) strains (also see below for strain construction).

To integrate *3GFP* or *3mCherry* at the 3' end of the chromosomal *CSE4* gene, we constructed two targeting vectors. For *3mCherry* tagging, we amplified a 3' end fragment of the *CSE4* gene corresponding to nucleotides 41-687 from genomic DNA using a forward primer flanked with a SalI site and a reverse primer flanked with BamHI site. This PCR fragment was digested with SalI and BamHI, and ligated into pRS303:*3mCherry* digested with SalI and BamHI, yielding pRS303:*CSE4*$_{41\text{-}687}$-*3mCherry*. For 3GFP tagging, an engineered BamHI-BglII *CSE4*$_{41\text{-}687}$ fragment was amplified from the genomic DNA, digested with BamHI and BglII, and ligated into pBS-3GFP-TRP1 digested with BamHI, yielding pBS-CSE4$_{41\text{-}687}$-3GFP-TRP1. Both *CSE4* inserts were verified by sequencing. See below for strain construction using these plasmids.

The *mCherry-TUB1* open reading frame was subcloned from pAK011 using XhoI and NotI, and ligated into pRS305 digested with XhoI and NotI to yield pRS305:*mCherry-TUB1*. To drive expression of *mCherry-TUB1*, an engineered SalI fragment containing the *MET3* promoter was amplified by PCR, digested with SalI, and ligated into pRS305:*mCherry-TUB1* digested with XhoI, to yield pRS305-*MET3*p:*mCherry-TUB1*.

Media and Strain Construction

All strains are derived from YWL36 or YWL37 [39] and listed in Table S1. We transformed yeast strains using the lithium acetate method [40]. Gene deletion and fluorescent protein tagged strains were constructed by PCR product-mediated transformation [41] or by mating and tetrad analysis. Transformants were clonally purified by streaking to individual colonies on selective media. Proper targeting was confirmed by PCR. At least two independent transformants were chosen from each tagging and disruption procedure for subsequent localization studies. Yeast synthetic defined (SD) media was obtained from Sunrise Science Products (San Diego, CA).

To construct the *TAIL-3GFP* strain, pSM01:*TAIL-3GFP* was digested with AflII and BsiWI, and the resulting 7.7 kb fragment was gel purified and transformed into a *dyn1*Δ strain (YWL520) to yield YWL714. To construct the *MOTOR-3YFP* strains, pSM01:*MOTOR-3YFP* (wild-type or mutants) was digested with BsaBI and BsiWI, and the resulting 11.7 kb fragment was gel purified and transformed into YWL520 to yield YWL733 (wild-type), YWL740 (K2424A) and YWL742 (E2488Q). To construct $DYN1_{K2424A}$*-3YFP*, pSM07:$DYN1_{K2424A}$*-3YFP* was linearized with BsiWI and transformed

into YWL614 to yield YWL830. Stable Trp^+ transformants were selected and then screened for proper integration into the *DYN1* locus by PCR.

To visualize microtubules, either pRS305-*MET3*p:*mCherry-TUB1* (*MET3p-mCherry-TUB1::LEU2*) or pAFS125C (*CFP-TUB1::URA*) [17, 22, 23] were digested with HindIII or StuI, respectively, and transformed into strains. Leu^+ or Ura^+ transformants, respectively, were selected and examined for mCherry-Tub1 or CFP-Tub1 fluorescence by microscopy.

To construct *JNM1-3mCherry* strains, chromosomal *JNM1* was initially tagged with *3mCherry::HIS3* in a wild-type (YWL36) strain to yield YWL869, which was then mated with YWL714 or YWL733. Sporulation and tetrad dissection of the resulting diploid strains yielded YWL899 and YWL894.

To construct the *CSE4-3mCherry* and *CSE4-3GFP* strains, pRS303:$CSE4_{41\text{-}687}$-*3mCherry* or pBS-$CSE4_{41\text{-}687}$-*3GFP-TRP1*, respectively, was linearized with EcoRV, which digests at nucleotide 205 within the *CSE4* gene, and transformed into YWL37 to yield YWL999 (*CSE4-3mCherry::HIS3*) and YWL980 (*CSE4-3GFP::TRP1*). Null mutation of *cse4* is inviable. Strains expressing Cse4-3mCherry or Cse4-3GFP as their sole source of Cse4 were viable, indicating that the tagged proteins were functional.

Image Acquisition

Yeast cultures were grown to mid-log phase at 30°C and analyzed on an agarose pad containing nonfluorescent SD media. Wide-field fluorescence images were collected using a 1.49 NA 100X objective on a Nikon 80i upright microscope equipped with piezo Z-control (Physik Instrumente), electronically controlled SmartShutter (Sutter

Instrument), motorized filter cube turret, and a cooled EM-CCD Cascade-II camera (Photometrics). Microscope system was controlled by NIS-Elements software (Nikon). Sputtered/ET filter cube sets (Chroma Technology) were used for imaging CFP (49001), GFP (49002), YFP (49003), and mCherry (49008) fluorescence. For Cse4-standardized ratiometric measurements, strains were imaged using a 1.45 NA 100X objective on a Nikon TE2000E inverted microscope equipped with a cooled EM-CCD iXon^{EM} camera (Andor Technology). Using ImageJ, we drew a circle encompassing 3 X 3 pixels to quantify the intensities of the plus-end foci of motor-3YFP, Dyn1/HC-3mCherry, and Dyn1/HC-3GFP. For FRET experiments, images were collected using a 1.30 NA 100X objective on an LSM 510 NLO upright confocal microscope (Zeiss) equipped with 543 nm HeNe laser and 488 nm argon laser line, and controlled by Zen 2007 software (Central Microscopy Facility, Marine Biological Laboratory, Woods Hole). For each strain, single focal plane images (1.2 μm optical thickness) of mCherry fluorescence (λ > 560 nm) upon λ = 543 nm excitation was captured first, followed by FRET fluorescence (λ > 560 nm) and GFP fluorescence (λ = 505-545 nm) upon λ = 488 nm excitation. Intensities of foci were quantified using ImageJ and corrected for background fluorescence locally, as described [25, 39]. The spillover of fluorescence emission into the FRET channel (*i.e.*, the background fluorescence in the FRET channel due to direct excitation of 3GFP and mCherry instead of intermolecular FRET) was determined by capturing images of strains expressing Num1-mCherry (YWL644) or tail-3GFP alone (YWL714). $FRET_R$ value, the relative increase of fluorescence emission detected in the FRET channel (when both proteins were co-expressed; YWL843) over the expected background from spillover fluorescence, was calculated accordingly as described [25].

Cell Lysis and Immunoblotting

Yeast cultures were grown to mid-log phase in 6 ml SD media and harvested. Cell pellets were resuspended in 0.2 ml of 0.1 M NaOH and incubated for 5 minutes at room temperature as described [42]. Following centrifugation, the resulting cell pellet was resuspended in sample buffer. Crude lysates were separated on a 4-15% gradient SDS-PAGE. Proteins were electroblotted to PVDF in 25 mM Tris, 192 mM glycine supplemented with 0.05% SDS and 10% methanol for 30 minutes. Rabbit anti-GFP polyclonal antibody (Invitrogen) and HRP-conjugated goat anti-rabbit antibody (Jackson ImmunoResearch Laboratories) were used at 1:500 and 1:3333 dilutions, respectively. Chemiluminescence signal was acquired and imaged using a G:BOX Chemi HR16 (Syngene) equipped with a 16-bit CCD camera (Sony ICX285AL; pixel size of 6.45 μm x 6.45 μm). Immunoblots were exposed (durations ranged from 10 s to 5 min) without saturating the camera's pixels.

Nocodazole Treatment and Diffusion Rate Estimates

To rule out the possibility that full-length dynein (Dyn1/HC-3GFP) is binding along the astral microtubules, we used the MT-depolymerizing drug, nocodazole, to disassemble the astral microtubules. In preliminary experiments using the conditions established by John Pringle's lab (Jacobs et al., 1988. JCB 107:1409), we found that 93% ± 2% of our wild-type cells contained no astral microtubules after a 60 min incubation in 20 μg/ml of nocodazole-containing medium (Fig. S1F). Using fluorescently-marked tubulin, we confirmed that the loss of astral microtubules occurred

by 10 min, and was in effect for the remaining 60 min period after the addition of nocodazole. This was similar to the observation reported by the Pringle lab. We scored for the presence of astral microtubules in each cell very conservatively; a linear structure of 3 pixels, corresponding to ~0.5 μm, was scored as an astral microtubule if it emanated from the SPB. The remaining 7% of nocodazole-treated cells all exhibited very short astral microtubules.

We next examined cortical targeting of tail-3GFP and Dyn1/HC-3GFP after 60 min of nocodazole treatment in *pac1*Δ mutant (to block binding along microtubules as well as binding to the plus-ends). Using microtubules marked by mCherry-Tub1, we also confirmed the unequivocal loss of astral microtubules in the *pac1*Δ cells after 60 min of nocodazole treatment, as observed for wild-type cells. We found that the likelihood of finding a cortical focus was significantly higher for tail-3GFP than Dyn1/HC-3GFP. While cortical tail-3GFP foci were observed in 61% ± 3% of cells, cortical Dyn1/HC-3GFP foci were observed in 2% ± 1% of cells (Fig. S1F; n > 160 in each case). These values are similar to the untreated control cells. If the difference in cortical association between tail and full-length dynein is due to the binding of Dyn1/HC-3GFP along the length of microtubules, then nocodazole disruption of astral microtubules should increase the population of Dyn1/HC-3GFP molecules that can associate with the cell cortex. The observed results in the presence and absence of nocodazole did not support this prediction for Dyn1/HC-3GFP (Fig. S1F). Thus, we conclude that Dyn1/HC-3GFP does not bind to the cortex in the absence of microtubules.

The conditions used in our nocodazole experiments account for the diffusion rate of Dyn1/HC-3GFP, as well as the difference in diffusion rate between tail complex and full-length dynein complex. Our reasoning is below.

First, we used the diffusion coefficient of 0.016 $\mu m^2/s$ – a value experimentally determined for axonemal dynein 1 complex purified from sea urchin (Gibbons and Fronk, 1979, JBC, 254:187) – to estimate the diffusion rate of yeast cytoplasmic dynein. We believe that this diffusion coefficient is a close approximation because yeast dynein complex (with a calculated MW of 1,156 kDa based on 2 copies each of Dyn1/HC, Pac11/IC, Dyn3/LIC, and Dyn2/LC) is about the same size as the sea urchin axonemal dynein 1 complex (with a measured MW of 1,260 kDa). Thus, while the true diffusion coefficient for yeast dynein complex may differ slightly due to differences in the hydrodynamic size and shape (yeast dynein is slightly smaller in MW), we believe that the value of 0.016 $\mu m^2/s$ may represent a lower boundary for our estimation (*i.e.*, yeast dynein may actually have a higher coefficient and diffuse faster). Assuming that yeast dynein complex diffuses at this rate, then it should be able to sample an area of 7 x 7 μm^2 within 51 min (a typical large budded yeast cell has 7 μm as the upper limit for its long-axis). Thus, a 60 min incubation time in nocodazole should be sufficient for the dynein complex to diffuse to the cell cortex.

Second, although diffusion coefficients between tail-3GFP and Dyn1/HC-3GFP are likely different due to size discrepancies, we believe this difference to be less significant *in vivo*. The tail domain likely dimerizes *in vivo* (Habura et al., 1999 JBC 274:15447; Tynan *et al.*, 2000 JBC 275: 32769). Also, our data for tail-3GFP suggest that it forms a complex with the accessory chains of dynein in the cell. For example,

Figure S2A shows that the localization of tail-3GFP depends on dynein subunits. This result is consistent with studies of vertebrate dynein showing that the tail domain contains binding sites for IC and LIC (Tynan et al, 2000, JBC 275: 32769). Therefore, we predict that the tail complex should be approximately 528 kDa (calculated based on 2 copies each for tail, Pac11/IC, Dyn3/LIC, and Dyn2/LC). Notably, this molecular weight is only ~2-fold smaller than that calculated for full-length dynein complex, a difference that cannot account for a 30-fold difference in cortical targeting of tail-3GFP compared to Dyn1/HC-3GFP in the absence of microtubules (Fig. S1F). Taken together, the data support the notion that Dyn1/HC-3GFP is masked from binding to the cell cortex independent of diffusion rate.

Additionally, previously published results have shown that cells lacking Bik1/Clip170 exhibited microtubule length defects (Sheeman *et al.*, Curr Biol. 2003, 13:364; Carvalho et al., Dev Cell. 2004, 6:815). Consistent with the published results, we observed that *bik1*Δ cells contained either short/unstable or no astral microtubules in our movie analysis. Using the same criteria for counting nocodazole-treated cells above, we quantified the percentage of *bik1*Δ cells with astral microtubules that are longer than 0.5 μm. We found that 26% of *bik1*Δ cells contained visible astral microtubules with >0.5 μm in length, while 74% contained no astral microtubules (Fig. S1F). If binding of Dyn1/HC-3GFP along the length of astral microtubules reduces the pool of dynein for binding to the cell cortex, then we would expect to observe more cortical Dyn1/HC-3GFP foci in *bik1*Δ mutant compared to wild-type strain. Our data did not support this prediction. Instead, our results in Figure 4C show that Dyn1/HC-3GFP is significantly reduced from the cortex. Additionally, Dyn1/HC-3GFP was significantly reduced from

the plus-ends in *bik1*Δ cells with visible astral microtubules. Taken together, these data provide a direct correlation for plus-end binding and cortical binding, which supports our proposed model that targeting of dynein to the plus-end unmasks the molecule for cortical binding.

Supplemental References

22. Lee, W.L., Oberle, J.R., and Cooper, J.A. (2003). The role of the lissencephaly protein Pac1 during nuclear migration in budding yeast. J. Cell Biol. 160, 355–364.

37. Sikorski, R.S., and Hieter, P. (1989). A system of shuttle vectors and yeast host strains designed for efficient manipulation of DNA in Saccharomyces cerevisiae. Genetics 122, 19–27.

17. Lee, W.L., Kaiser, M.A., and Cooper, J.A. (2005). The offloading model for dynein function: differential function of motor subunits. J. Cell Biol. 168, 201–207.

38. Weiner, M.P., Costa, G.L., Schoettlin, W., Cline, J., Mathur, E., and Bauer, J.C. (1994). Site-directed mutagenesis of double-stranded DNA by the polymerase chain reaction. Gene 151, 119–123.

39. Vorvis, C., Markus, S.M., and Lee, W.L. (2008). Photoactivatable GFP tagging cassettes for protein-tracking studies in the budding yeast Saccharomyces cerevisiae. Yeast 25, 651–659.

40. Knop, M., Siegers, K., Pereira, G., Zachariae, W., Winsor, B., Nasmyth, K., and Schiebel, E. (1999). Epitope tagging of yeast genes using a PCR-based strategy: more tags and improved practical routines. Yeast 15, 963–972.

41. Longtine, M.S., McKenzie, A., 3rd, Demarini, D.J., Shah, N.G., Wach, A., Brachat, A., Philippsen, P., and Pringle, J.R. (1998). Additional modules for versatile and economical PCR-based gene deletion and modification in Saccharomyces cerevisiae. Yeast 14, 953–961.

23. Moore, J.K., Li, J., and Cooper, J.A. (2008). Dynactin function in mitotic spindle positioning. Traffic 9, 510–527.

25. Muller, E.G., Snydsman, B.E., Novik, I., Hailey, D.W., Gestaut, D.R., Niemann, C.A., O'Toole, E.T., Giddings, T.H., Jr., Sundin, B.A., and Davis, T.N. (2005). The organization of the core proteins of the yeast spindle pole body. Mol. Biol. Cell 16, 3341–3352.

42. Kushnirov, V.V. (2000). Rapid and reliable protein extraction from yeast. Yeast 16, 857–860.

30. Reck-Peterson, S.L., Yildiz, A., Carter, A.P., Gennerich, A., Zhang, N., and Vale, R.D. (2006). Single-molecule analysis of dynein processivity and stepping behavior. Cell 126, 335–348.

11. Mocz, G., and Gibbons, I.R. (2001). Model for the motor component of dynein heavy chain based on homology to the AAA family of oligomeric ATPases. Structure 9, 93–103.

34. Meluh, P.B., Yang, P., Glowczewski, L., Koshland, D., and Smith, M.M. (1998). Cse4p is a component of the core centromere of Saccharomyces cerevisiae. Cell 94, 607–613.

35. Joglekar, A.P., Bouck, D.C., Molk, J.N., Bloom, K.S., and Salmon, E.D. (2006). Molecular architecture of a kinetochore-microtubule attachment site. Nat. Cell Biol. 8, 581–585.

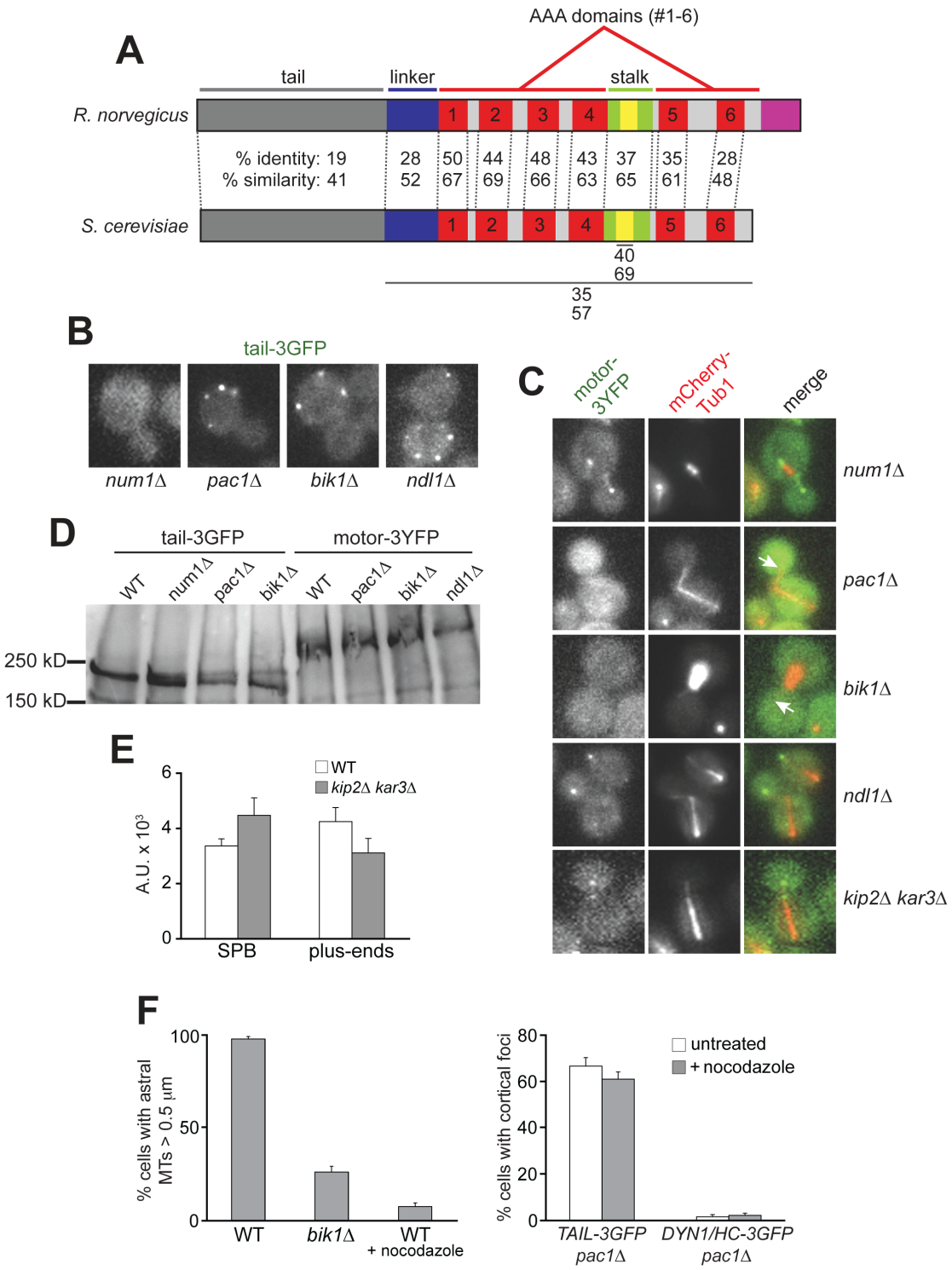

Figure S1. **(A) Domain homology between vertebrate and budding yeast cytoplasmic dynein heavy chains.** The boundary between the tail and linker domains was defined based on *in vitro* studies of Dyn1/HC [30]. AAA domain boundaries were as described [11]. Percent identity and similarity were determined using the BLAST protein

alignment algorithm ('bl2seq') and the BLOSUM62 matrix to score alignment. **(B)-(D) Localization of tail and motor domains in null strains.** Representative images used for quantification in Figure 4 and S2B. For two-color merge in (C), mCherry-Tub1 is displayed in red and motor-3YFP is in green. Each image is a 2 μm Z-stack of wide-field images. Arrows indicate plus-ends lacking motor-3YFP signal. (D) Western blot of wild-type and null strains carrying *TAIL-3GFP* and *MOTOR-3YFP*. Equal amount of total cell lysate was loaded in each lane, transferred to PVDF and probed with anti-GFP antibodies. **(E) Quantification of fluorescence intensities of SPB and plus-end associated motor-3YFP foci in *kip2*Δ *kar3*Δ cells relative to wild-type.** Fields containing a mixed population of both strains were imaged simultaneously to ensure identical imaging conditions. Movies were analyzed for foci at SPB (n > 10) and plus-ends (n > 15), which were identified using CFP-Tub1 or mCherry-Tub1. Error bars represent standard error. **(F) The different capacities of tail-3GFP and Dyn1/HC-3GFP to associate with the cell cortex is not due to the latter's ability to bind along astral microtubules.** Since Dyn1/HC can bind microtubules via its microtubule-binding domain, we tested whether differences in cortical association observed between tail-3GFP and Dyn1/HC-3GFP are due to this property. (*LEFT*) Deletion of *BIK1/CLIP-170* or treatment with nocodazole reduces astral microtubule numbers (n > 130). Nocodazole (20 μg/ml supplemented with 1% DMSO) was added to log-phase cultures, which were then grown at 25ºC in synthetic defined media for 1 hour. After 10 minutes of treatment, astral microtubules were reduced by ~92% with respect to untreated cells, but gradually returned after 2 hours (not shown). (*RIGHT*) Time-lapse fluorescence microscopy followed by foci-counting revealed no differences in cortical association between tail-3GFP and Dyn1/HC-3GFP after one hour of nocodazole treatment (n > 160).

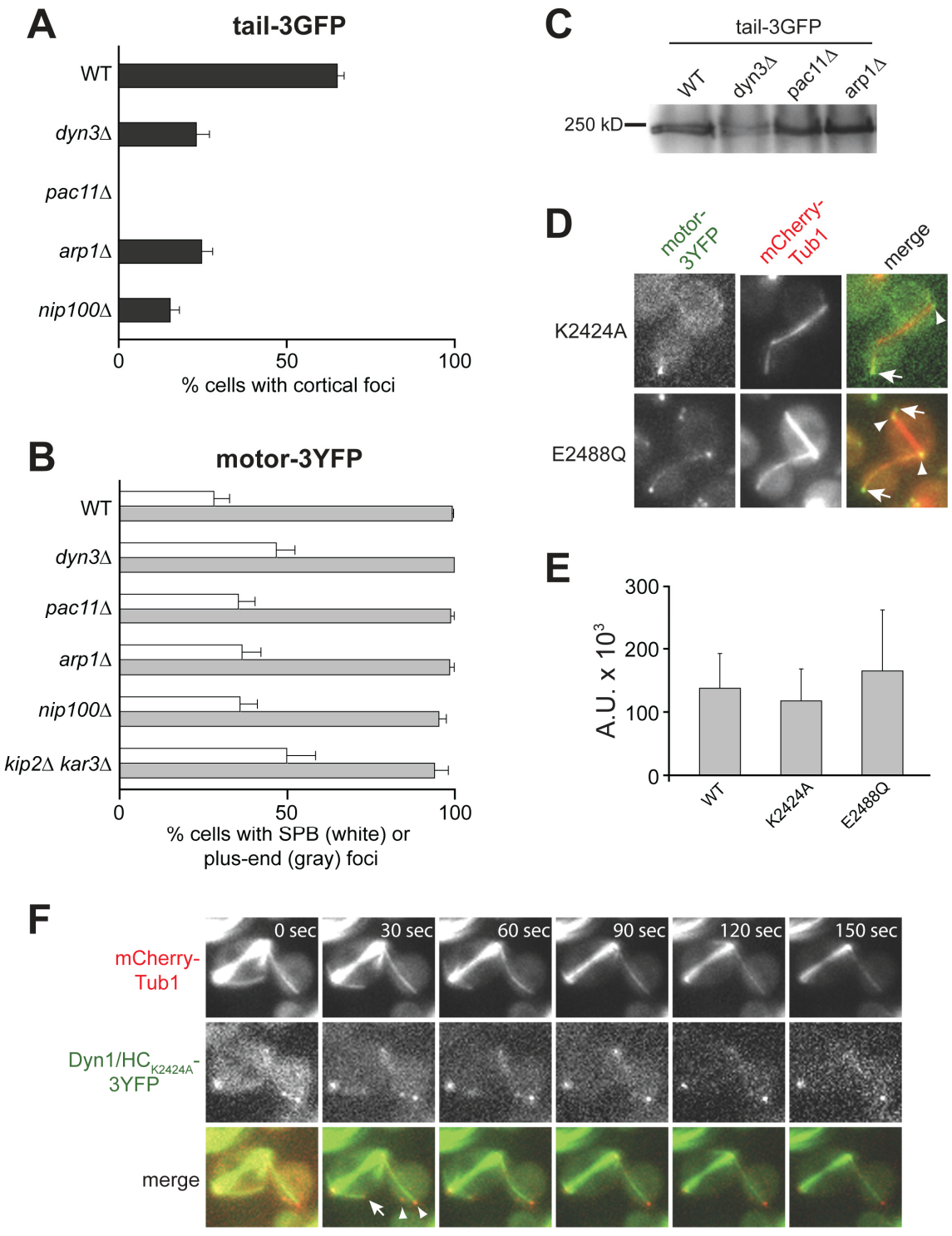

Figure S2. **(A)-(C) Localization of tail-3GFP and motor-3YFP in null mutants.** The percentage of cells that display (A) tail-3GFP or (B) motor-3YFP foci at a given subcellular site is plotted for different null mutants (n > 100 cells counted for each strain). To identify foci at the cortex, SPB, and plus-end, a 2 μm Z-stack of images was

collected at 5 s intervals for each null strain expressing mCherry-Tub1 and either tail-3GFP or motor-3YFP. Movies were analyzed for foci at indicated locations. Error bars represent standard error of proportion. (C) Western blot of wild-type and null strains carrying *TAIL-3GFP*. Equal amount of total cell lysate was loaded in each lane, transferred to PVDF and probed with anti-GFP antibodies. **(D)-(E) Mutations in AAA3 do not affect SPB or plus-end targeting of the motor domain.** (D) Maximum intensity projections of wide-field images of cells expressing motor-3YFP AAA3 mutants (as indicated) under the control of the endogenous *DYN1* promoter and mCherry-Tub1 under the control of the *MET3* promoter. Merged image on the right depicts motor-3YFP mutants in green and mCherry-Tub1 in red. Arrows indicate plus-end foci; arrowheads indicate SPB foci. (E) Quantification of fluorescence intensities (A. U.) of plus-end foci of motor-3YFP mutants relative to wild-type (n > 30 foci). **(F) Dyn1/HC$_{K2424A}$ mutant is targeted to the SPB, plus-ends and the cell cortex from where it stably attaches to astral microtubules.** Representative movie frames of Dyn1/HC$_{K2424A}$-3YFP and mCherry-Tub1 depicting Dyn1/HC$_{K2424A}$-3YFP at the SPB, microtubule plus-end and the cell cortex. Each image is a maximum intensity projection of a 2 μm Z-stack of wide-field images. The time elapsed in seconds is indicated (also see Movie S7).

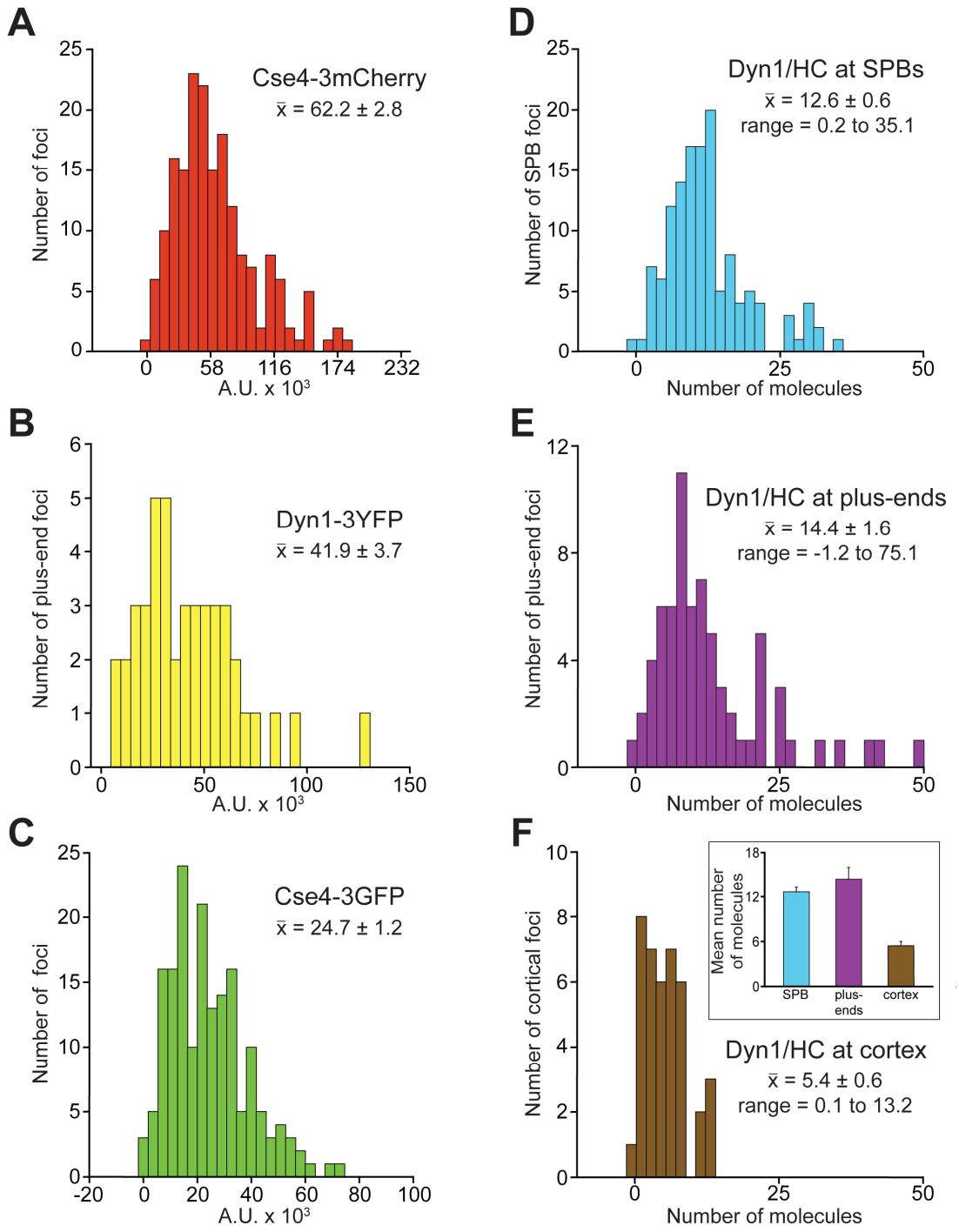

Figure S3. **(A)-(C) Fluorescence intensity histograms of Cse4-3mCherry, Dyn1/HC-3YFP and Cse4-3GFP.** Histograms of fluorescence intensity of individual foci of (A) Cse4-3mCherry (n = 180), (B) plus-end Dyn1/HC-3YFP (n = 43), and (C) Cse4-3GFP (n = 173) in wild-type cells. Fields containing a mixed population of strains were imaged simultaneously to ensure identical imaging conditions. Mean values from these data sets were used for standardizing the intensity distribution of Dyn1/HC-3mCherry, motor-

3YFP, and Dyn1/HC-3GFP in *num1*Δ in Figure 5 to number of molecules. **(D)-(F) Quantitative ratiometric measurements of Dyn1/HC at SPBs, plus-ends and the cell cortex.** Histograms of the numbers of molecules of Dyn1/HC-3mCherry or Dyn1/HC-3GFP per (D) SPB (n = 132), (E) plus-end (n = 71), or (F) cortical focus (n = 40) in wild-type cells. For (D) and (E), fields containing a mixed population of strains expressing Cse4-3mCherry only or Dyn1/HC-3mCherry with CFP-Tub1 were imaged simultaneously to ensure identical imaging conditions. The mean fluorescence intensity of Cse4-3mCherry was assigned a value of 32 molecules of 3mCherry [34, 35] and was used to normalize Dyn1/HC-3mCherry fluorescence intensity (A.U.) to number of molecules. For (F), cells expressing Dyn1/HC-3GFP and mCherry-Tub1 were imaged. We used the intensity distribution of Dyn1/HC-3GFP at plus-ends as a standard (data not shown), which was normalized using the mean value of 14.4 copies of Dyn1/HC per plus-end, as determined for Dyn1/HC-3mCherry in (E). Inset graph in (F) depicts the mean number of molecules for (D), (E) and (F) with standard error. Plus-end foci were identified with either CFP-Tub1 or mCherry-Tub1.

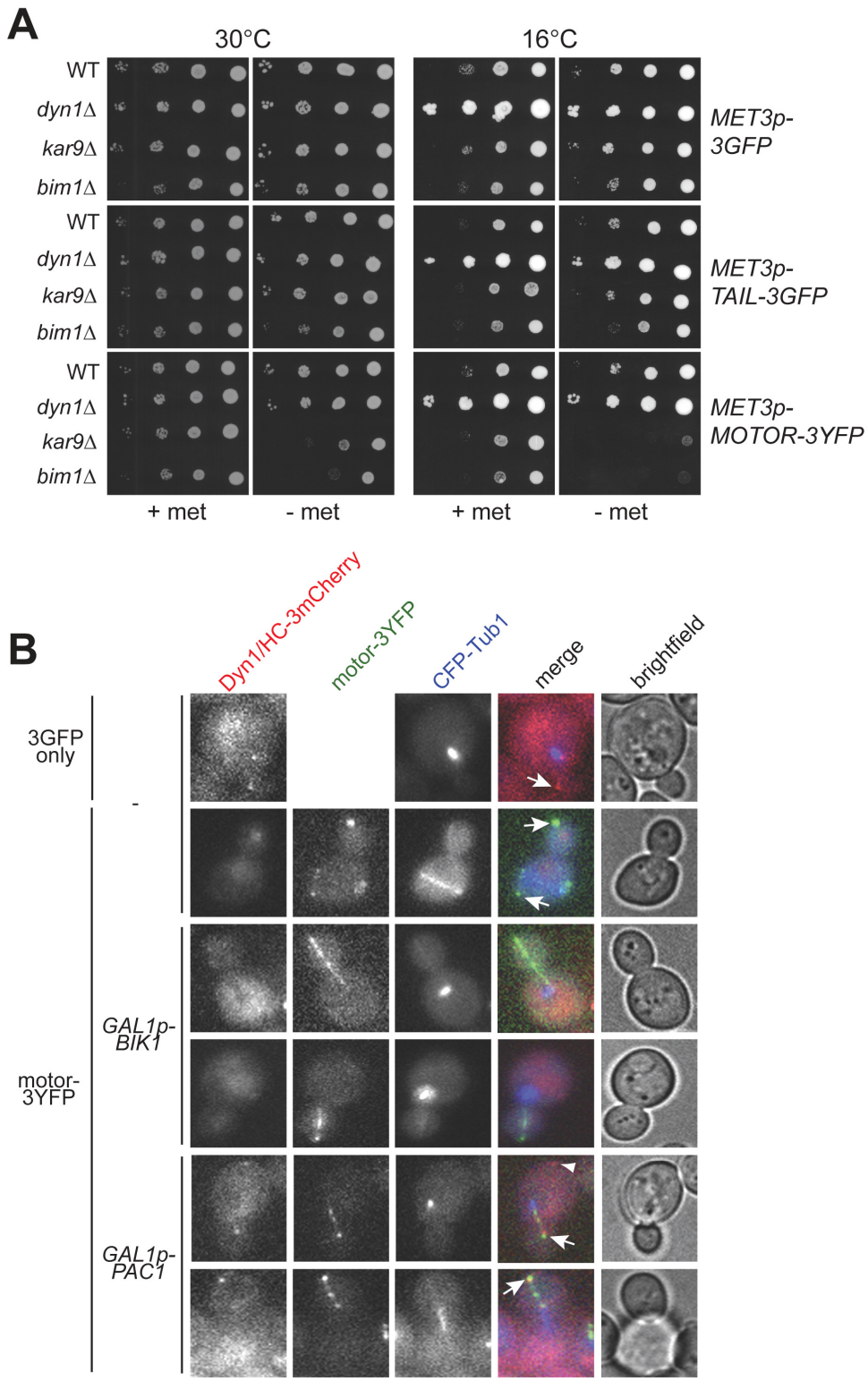

Figure S4. **(A) Isolated motor domain induces synthetic growth defects in *kar9*Δ and *bim1*Δ mutants.** WT, *dyn1*Δ, *kar9*Δ or *bim1*Δ strains were transformed with plasmids containing either *3GFP*, *TAIL-3GFP* or *MOTOR-3YFP* under the control of the

inducible *MET3* promoter (pRS315-*MET3p*). Strains were grown to mid-log phase in SD-Leu media supplemented with 1 g/L methionine (to repress the *MET3* promoter). Ten-fold serial dilutions were plated on SD-Leu media (dilution series from right to left in each panel) with or without methionine, and grown at 30°C for 2 days, or 16°C for 14 days. **(B) Dyn1/HC-3mCherry targeting in the presence of motor-3YFP is restored by overexpression of Pac1/LIS1.** Representative images used for quantification in Figure 6D. For three-color merge, motor-3YFP is depicted in green, Dyn1/HC-3mCherry in red and CFP-Tub1 in blue. Arrows indicate plus-end foci; arrowhead indicates cortical focus.

Table S1. Strains used in this study.

Strain	Genotype	Source
YWL36	*Mata ura3-52 lys2-801 leu2-Δ1 his3-Δ200 trp1-Δ63*	[39]
YWL37	*Matα ura3-52 lys2-801 leu2-Δ1 his3-Δ200 trp1-Δ63*	[39]
YWL271	*Matα DYN1-3YFP::TRP ura3-52 lys2-801 leu2-Δ1 his3-Δ200 trp1-Δ63*	[17]
YWL395	*Matα DYN1-3GFP::TRP1 ura3-52::URA3-CFP-TUB1 bik1Δ::HIS3 lys2-801 leu2-Δ1 his3-Δ200 trp1-Δ63*	This study
YWL401	*Matα DYN1-3GFP::TRP1 ura3-52::URA3-CFP-TUB1 pac1Δ::HIS3 lys2-801 leu2-Δ1 his3-Δ200 trp1-Δ63*	This study
YWL434	*Mata DYN1-3GFP::TRP1 ura3-52::URA3-CFP-TUB1 lys2-801 leu2-Δ1 his3-Δ200 trp1-Δ63*	This study
YWL520	*Matα dyn1Δ::HIS3 ura3-52 lys2-801 leu2-Δ1 his3-Δ200 trp1-Δ63*	This study
YWL614	*Matα dyn1Δ::HIS3 TUB1::MET3p-mCherry-TUB1::LEU2 ura3-52 lys2-801 leu2-Δ1 his3-Δ200 trp1-Δ63*	This study
YWL644	*Mata NUM1-mCherry::HIS3 ura3-52 lys2-801 leu2-Δ1 his3-Δ200 trp1-Δ63*	This study
YWL677	*Matα MOTOR$_{K2424A}$-3YFP::TRP1 TUB1::MET3p-mCherry-TUB1::LEU2 ura3-52 lys2-801 leu2-Δ1 his3-Δ200 trp1-Δ63*	This study
YWL679	*Matα MOTOR$_{E2488Q}$-3YFP::TRP1 TUB1::MET3p-mCherry-TUB1::LEU2 ura3-52 lys2-801 leu2-Δ1 his3-Δ200 trp1-Δ63*	This study
YWL714	*Matα TAIL-3GFP::TRP ura3-52 lys2-801 leu2-Δ1 his3-Δ200 trp1-Δ63*	This study
YWL731	*Mata DYN1-2mCherry::HIS3 ura3-52::URA3-CFP-TUB1 lys2-801 leu2-Δ1 his3-Δ200 trp1-Δ63*	This study
YWL733	*Matα MOTOR-3YFP::TRP ura3-52 lys2-801 leu2-Δ1 his3-Δ200 trp1-Δ63*	This study
YWL770	*Mata/α DYN1-2mCherry::HIS3/TAIL-3GFP::TRP ura3-52::URA3-CFP-TUB1/ura3-52 lys2-801/lys2-801 leu2-Δ1/leu2-Δ1 his3-Δ200/his3-Δ200 trp1-Δ63/trp1-Δ63*	This study
YWL771	*Mata/α DYN1-2mCherry::HIS3/MOTOR-3YFP::TRP ura3-52::URA3-CFP-TUB1/ura3-52 lys2-801/lys2-801 leu2-Δ1/leu2-Δ1 his3-Δ200/his3-Δ200 trp1-Δ63/trp1-Δ63*	This study
YWL773	*Mata/α DYN1-2mCherry::HIS3/MOTOR$_{K2424A}$-3YFP::TRP ura3-52::URA3-CFP-TUB1/ura3-52 lys2-801/lys2-801 leu2-Δ1/leu2-Δ1 his3-Δ200/his3-Δ200 trp1-Δ63/trp1-Δ63*	This study
YWL774	*Mata/α DYN1-2mCherry::HIS3/MOTOR$_{E2488Q}$-3YFP::TRP ura3-52::URA3-CFP-TUB1/ura3-52lys2-801/lys2-801 leu2-Δ1/leu2-Δ1 his3-Δ200/his3-Δ200 trp1-Δ63/trp1-Δ63*	This study

YWL775	*Mata/α DYN1-2mCherry::HIS3/3GFP::TRP ura3-52::URA3-CFP-TUB1/ura3-52 lys2-801/lys2-801 leu2-Δ1/leu2-Δ1 his3-Δ200/his3-Δ200 trp1-Δ63/trp1-Δ63*	This study
YWL788	*Mata DYN1-3YFP::TRP ura3-52::URA3-CFP-TUB1 lys2-801 leu2-Δ1 his3-Δ200 trp1-Δ63*	This study
YWL827	*Matα TAIL-3GFP::TRP pac11Δ::KAN^R TUB1::MET3p-mCherry-Tub1::LEU2 ura3-52 lys2-801 leu2-Δ1 his3-Δ200 trp1-Δ63*	This study
YWL830	*Matα dyn1Δ::HIS3::DYN1$_{K2424A}$-3YFP::TRP TUB1::MET3p-mCherry-TUB1::LEU2 ura3-52 lys2-801 leu2-Δ1 his3-Δ200 trp1-Δ63*	This study
YWL831	*Matα TAIL-3GFP::TRP arp1Δ::HIS3 TUB1::MET3p-mCherry-Tub1::LEU2 ura3-52 lys2-801 leu2-Δ1 his3-Δ200 trp1-Δ63*	This study
YWL832	*Matα TAIL-3GFP::TRP nip100Δ::HIS3 TUB1::MET3p-mCherry-Tub1::LEU2 ura3-52 lys2-801 leu2-Δ1 his3-Δ200 trp1-Δ63*	This study
YWL833	*Mata TAIL-3GFP::TRP num1Δ::KAN^R TUB1::MET3p-mCherry-Tub1::LEU2 ura3-52 lys2-801 leu2-Δ1 his3-Δ200 trp1-Δ63*	This study
YWL834	*Matα TAIL-3GFP::TRP dyn3Δ::KAN^R TUB1::MET3p-mCherry-Tub1::LEU2 ura3-52 lys2-801 leu2-Δ1 his3-Δ200 trp1-Δ63*	This study
YWL841	*Matα TAIL-3GFP::TRP1 TUB1::MET3p-mCherry-TUB1::LEU2 ura3-52 lys2-801 leu2-Δ1 his3-Δ200 trp1-Δ63*	This study
YWL843	*Matα TAIL-3GFP::TRP NUM1-mCherry::HIS3 ura3-52 lys2-801 leu2-Δ1 his3-Δ200 trp1-Δ63*	This study
YWL845	*Matα MOTOR-3YFP::TRP TUB1::MET3p-mCherry-Tub1::LEU2 ura3-52 lys2-801 leu2-Δ1 his3-Δ200 trp1-Δ63*	This study
YWL847	*Matα MOTOR-3YFP::TRP pac11Δ::KAN^R TUB1::MET3p-mCherry-Tub1::LEU2 ura3-52 lys2-801 leu2-Δ1 his3-Δ200 trp1-Δ63*	This study
YWL848	*Matα MOTOR-3YFP::TRP nip100Δ::HIS3 TUB1::MET3p-mCherry-Tub1::LEU2 ura3-52 lys2-801 leu2-Δ1 his3-Δ200 trp1-Δ63*	This study
YWL849	*Matα MOTOR-3YFP::TRP arp1Δ::HIS3 TUB1::MET3p-mCherry-Tub1::LEU2 ura3-52 lys2-801 leu2-Δ1 his3-Δ200 trp1-Δ63*	This study
YWL850	*Matα MOTOR-3YFP::TRP num1Δ::KAN^R TUB1::MET3p-mCherry-Tub1::LEU2 ura3-52 lys2-801 leu2-Δ1 his3-Δ200 trp1-Δ63*	This study

YWL851	*Matα MOTOR-3YFP::TRP dyn3Δ::KAN^R TUB1::MET3p-mCherry-Tub1::LEU2 ura3-52 lys2-801 leu2-Δ1 his3-Δ200 trp1-Δ63*	This study
YWL864	*Mata/α dyn1Δ::HIS3/3GFP::TRP ura3-52::URA3-CFP-TUB1/ura3-52 lys2-801/lys2-801 leu2-Δ1/leu2-Δ1 his3-Δ200/his3-Δ200 trp1-Δ63/trp1-Δ63*	This study
YWL866	*Matα TAIL-3GFP::TRP bik1Δ::HIS3 TUB1::MET3p-mCherry-Tub1::LEU2 ura3-52 lys2-801 leu2-Δ1 his3-Δ200 trp1-Δ63*	This study
YWL869	*Mata JNM1-3mCherry::HIS3 ura3-52 lys2-801 leu2-Δ1 his3-Δ200 trp1-Δ63*	This study
YWL872	*Matα TAIL-3GFP::TRP pac1Δ::HIS3 TUB1::MET3p-mCherry-Tub1::LEU2 ura3-52 lys2-801 leu2-Δ1 his3-Δ200 trp1-Δ63*	This study
YWL874	*Matα MOTOR-3YFP::TRP pac1Δ::HIS3 TUB1::MET3p-mCherry-Tub1::LEU2 ura3-52 lys2-801 leu2-Δ1 his3-Δ200 trp1-Δ63*	This study
YWL876	*Matα MOTOR-3YFP::TRP bik1Δ::HIS3 TUB1::MET3p-mCherry-Tub1::LEU2 ura3-52 lys2-801 leu2-Δ1 his3-Δ200 trp1-Δ63*	This study
YWL881	*Matα TAIL-3GFP::TRP ndl1Δ::HIS3 TUB1::MET3p-mCherry-Tub1::LEU2 ura3-52 lys2-801 leu2-Δ1 his3-Δ200 trp1-Δ63*	This study
YWL883	*Matα MOTOR-3YFP::TRP ndl1Δ::HIS3 TUB1::MET3p-mCherry-Tub1::LEU2 ura3-52 lys2-801 leu2-Δ1 his3-Δ200 trp1-Δ63*	This study
YWL894	*Mata MOTOR-3YFP::TRP JNM1-3mCherry::HIS3 ura3-52 lys2-801 leu2-Δ1 his3-Δ200 trp1-Δ63*	This study
YWL898	*Mata DYN1-3mCherry::HIS3 ura3-52::URA3-CFP-TUB1 lys2-801 leu2-Δ1 his3-Δ200 trp1-Δ63*	This study
YWL899	*Matα TAIL-3GFP::TRP JNM1-3mCherry::HIS3 ura3-52 lys2-801 leu2-Δ1 his3-Δ200 trp1-Δ63*	This study
YWL903	*Mata/α DYN1-3mCherry::HIS3/3GFP::TRP1 ura3-52::URA3-CFP-TUB1/ura3-52 lys2-801/lys2-801 leu2-Δ1/leu2-Δ1 his3-Δ200/his3-Δ200 trp1-Δ63/trp1-Δ63*	This study
YWL904	*Mata/α DYN1-3mCherry::HIS3/TAIL-3GFP::TRP1 ura3-52::URA3-CFP-TUB1/ura3-52 lys2-801/lys2-801 leu2-Δ1/leu2-Δ1 his3-Δ200/his3-Δ200 trp1-Δ63/trp1-Δ63*	This study
YWL905	*Mata/α DYN1-3mCherry::HIS3/MOTOR-3YFP::TRP1 ura3-52::URA3-CFP-TUB1/ura3-52 lys2-801/lys2-801 leu2-Δ1/leu2-Δ1 his3-Δ200/his3-Δ200 trp1-Δ63/trp1-Δ63*	This study

YWL919	*Mata/α DYN1-3mCherry::HIS3/MOTOR$_{E2488Q}$-3YFP::TRP1 ura3-52::URA3-CFP-TUB1/ura3-52 lys2-801/lys2-801 leu2-Δ1/leu2-Δ1 his3-Δ200/his3-Δ200 trp1-Δ63/trp1-Δ63*	This study
YWL920	*Mata/α DYN1-3mCherry::HIS3/MOTOR$_{K2424A}$-3YFP::TRP1 ura3-52::URA3-CFP-TUB1/ura3-52 lys2-801/lys2-801 leu2-Δ1/leu2-Δ1 his3-Δ200/his3-Δ200 trp1-Δ63/trp1-Δ63*	This study
YWL953	*Mata/α DYN1-3mCherry::HIS3/MOTOR-3YFP::TRP1 KAN^R::GAL1p-BIK1 ura3-52::URA3-CFP-TUB1/ura3-52 lys2-801/lys2-801 leu2-Δ1/leu2-Δ1 his3-Δ200/his3-Δ200 trp1-Δ63/trp1-Δ63*	This study
YWL956	*Mata/α DYN1-3mCherry::HIS3/MOTOR-3YFP::TRP1 KAN::GAL1p-PAC1 ura3-52::URA3-CFP-TUB1/ura3-52 lys2-801/lys2-801 leu2-Δ1/leu2-Δ1 his3-Δ200/his3-Δ200 trp1-Δ63/trp1-Δ63*	This study
YWL980	*Matα CSE4-3GFP::TRP ura3-52 lys2-801 leu2-Δ1 his3-Δ200 trp1-Δ63*	This study
YWL999	*Mata CSE4-3mCherry::HIS3 ura3-52 lys2-801 leu2-Δ1 his3-Δ200 trp1-Δ63*	This study
YWL1001	*Matα DYN1-3GFP::TRP TUB1::MET3p-mCherry-TUB1::LEU2 num1Δ::HIS3 ura3-52 lys2-801 leu2-Δ1 his3-Δ200 trp1-Δ63*	This study
YWL1025	*Matα ura3-52 lys2-801 leu2-Δ1 his3-Δ200 trp1-Δ63 [MET3p-3GFP::LEU2, CEN]*	This study
YWL1026	*Matα ura3-52 lys2-801 leu2-Δ1 his3-Δ200 trp1-Δ63 [MET3p-TAIL-3GFP::LEU2, CEN]*	This study
YWL1027	*Matα ura3-52 lys2-801 leu2-Δ1 his3-Δ200 trp1-Δ63 [MET3p-MOTOR-3YFP::LEU2, CEN]*	This study
YWL1028	*Matα dyn1Δ::TRP ura3-52 lys2-801 leu2-Δ1 his3-Δ200 trp1-Δ63 [MET3p-3GFP::LEU2, CEN]*	This study
YWL1029	*Matα dyn1Δ::TRP ura3-52 lys2-801 leu2-Δ1 his3-Δ200 trp1-Δ63 [MET3p-TAIL-3GFP::LEU2, CEN]*	This study
YWL1030	*Matα dyn1Δ::TRP ura3-52 lys2-801 leu2-Δ1 his3-Δ200 trp1-Δ63 [MET3p-MOTOR-3YFP::LEU2, CEN]*	This study
YWL1031	*Matα kar9Δ::KAN^R ura3-52 lys2-801 leu2-Δ1 his3-Δ200 trp1-Δ63 [MET3p-3GFP::LEU2, CEN]*	This study
YWL1032	*Matα kar9Δ::KAN^R ura3-52 lys2-801 leu2-Δ1 his3-Δ200 trp1-Δ63 [MET3p-TAIL-3GFP::LEU2, CEN]*	This study
YWL1033	*Matα kar9Δ::KAN^R ura3-52 lys2-801 leu2-Δ1 his3-Δ200 trp1-Δ63 [MET3p-MOTOR-3YFP::LEU2, CEN]*	This study
YWL1034	*Matα bim1Δ::KAN^R ura3-52 lys2-801 leu2-Δ1 his3-Δ200 trp1-Δ63 [MET3p-3GFP::LEU2, CEN]*	This study

YWL1035	*Matα bim1Δ::KAN^R ura3-52 lys2-801 leu2-Δ1 his3-Δ200 trp1-Δ63 [MET3p-TAIL-3GFP::LEU2, CEN]*	This study
YWL1036	*Matα bim1Δ::KAN^R ura3-52 lys2-801 leu2-Δ1 his3-Δ200 trp1-Δ63 [MET3p-MOTOR-3YFP::LEU2, CEN]*	This study
YWL1075	*Mata JNM1-3mCherry::HIS3 ura3-52::URA3-CFP-TUB1 lys2-801 leu2-Δ1 his3-Δ200 trp1-Δ63*	This study
YWL1270	*Matα MOTOR-3YFP::TRP kip2Δ::KAN^R kar3Δ::HIS3 TUB1::MET3p-mCherry-Tub1::LEU2 ura3-52 lys2-801 leu2-Δ1 his3-Δ200 trp1-Δ63*	This study
YWL1277	*Matα DYN1-3GFP::TRP1 TUB1::MET3p-mCherry-TUB1::LEU2 ura3-52 lys2-801 leu2-Δ1 his3-Δ200 trp1-Δ63*	This study